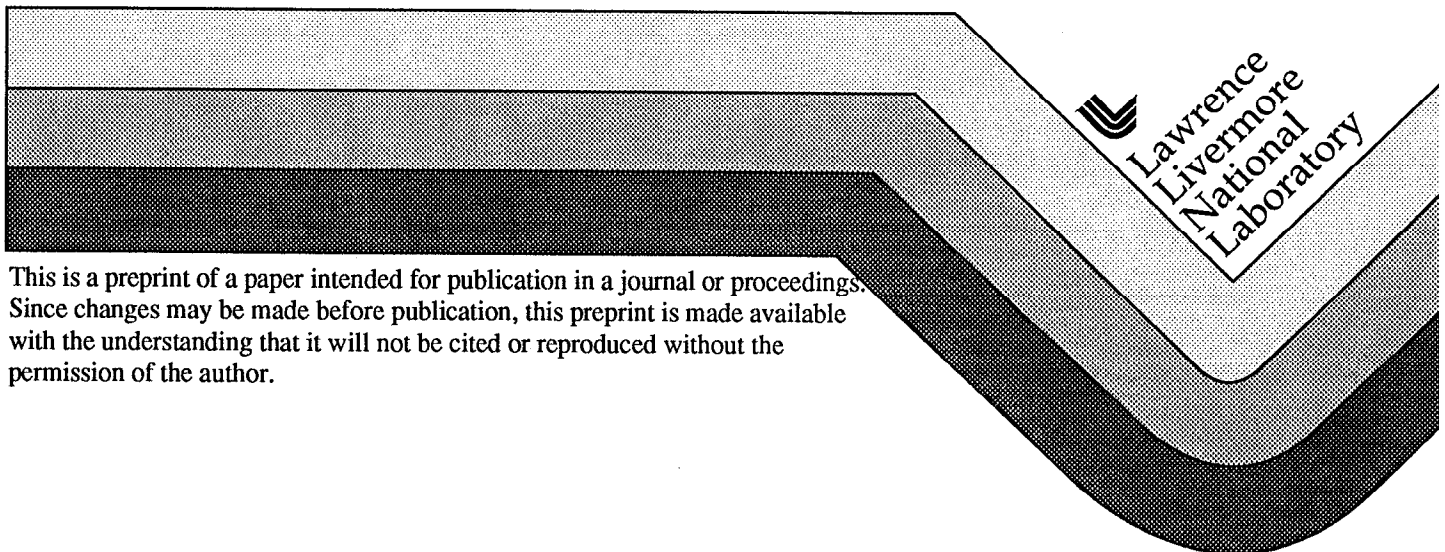# Delamination Detection in Reinforced Concrete Using Thermal Inertia

Nancy K. Del Grande
Philip F. Durbin

This paper was prepared for submittal to
Nondestructive Evaluation of Bridges and Highways II
Newport Beach, CA
March 3-5, 1999

November 30, 1998

Lawrence Livermore National Laboratory

DISCLAIMER

Delamination detection in reinforced concrete using thermal inertia

Nancy K. Del Grande[*] and Philip F. Durbin

Lawrence Livermore National Laboratory, MS L333, P. O. Box 808, Livermore, CA 94550

ABSTRACT

We investigated the feasibility of thermal inertia mapping for bridge deck inspections. Using pulsed thermal imaging, we heat-stimulated surrogate delaminations in reinforced concrete and asphalt-concrete slabs. Using a dual-band infrared camera system, we measured thermal inertia responses of Styrofoam implants under 5 cm of asphalt, 5 cm of concrete, and 10 cm of asphalt and concrete. We compared thermal maps from solar-heated concrete and asphalt-concrete slabs with thermal inertia maps from flash-heated concrete and asphalt-concrete slabs. Thermal inertia mapping is a tool for visualizing and quantifying subsurface defects. Physically, thermal inertia is a measure of the resistance of the bridge deck to temperature change. Experimentally, it is determined from the inverse slope of the surface temperature versus the inverse square root of time. Mathematically, thermal inertia is the square root of the product of thermal conductivity, density, and heat capacity. Thermal inertia mapping distinguishes delaminated decks which have below-average thermal inertias from normal or shaded decks.

Key Words: Pulsed Thermal Imaging, Thermal Inertia, Detection Of Concrete Bridgedeck Delaminations

1. INTRODUCTION

To date, most bridge inspections rely on human interpretation of surface visual features or chain dragging. These methods are slow, disruptive, unreliable and raise serious safety concerns. Single-band infrared (SBIR) thermal imaging, often referred to as thermography, is a technique with a promising potential. This technique has been used previously to detect structural deficiencies called delaminations within bridge decks. [1-4] However, it is difficult to distinguish subsurface delaminations from surface features on SBIR images. To locate and identify subsurface delaminations, we must first remove the mask from surface clutter (or unwanted detail on the IR images). Clutter is often introduced by foreign materials on the roadway, shadows, and reflected IR backgrounds.

Previous investigators have used video cameras, first to identify and then to remove surface-object clutter. Unlike thermal signals produced by subsurface delaminations, clutter signals vary with IR wavelength. To take advantage of this important spectral difference, the Lawrence Livermore National Laboratory (LLNL) applies dual-band infrared (DBIR) thermal and thermal inertia imaging for bridge inspections. DBIR thermal imaging allows precise, temperature measurement to reliably locate bridge deck delaminations by removing wavelength-dependent surface clutter from foreign materials. Thermal inertia imaging measures the bulk deck resistance to temperature change which decreases significantly at delamination sites.

The LLNL has successfully demonstrated the patented DBIR thermal and thermal inertia imaging methods[5,6] for a variety of applications. By removing spatially varying emissivity noise, DBIR methods typically improve temperature accuracy and precision by an order of magnitude compared to SBIR methods. In addition to precise temperature maps, DBIR methods provide emissivity-noise maps which clarify interpretation of heat flow anomalies from subsurface features, e.g., underground objects and structural deficiencies. Previously reported applications of DBIR imaging depicted:

- Geothermal aquifers under 6 to 60 meters of dry soil,[7,8]
- Cemetery walls, trenches and a building foundation under 80 cm of asphalt and debris[9]
- Buried mines, rocks and objects under 1 to 20 cm of disturbed sand, soil, or sod,[9-15]
- Airframe material loss from corrosion under 1 or 2 mm of exposed aluminum skin[15-23]
- Synthetic bridge-deck delaminations, 5 and 10 cm deep, in concrete and asphalt-concrete slabs [22-25]
- Bridge delaminations recorded from a mobile inspection laboratory and later confirmed by pavement removal [26-28]

[*] Correspondence: Email: delgrande1@llnl.gov; Telephone: 925 422-1010; Fax: 925 422-3834

2. FEASIBILITY STUDY USING SURROGATE BRIDGE DECKS

A feasibility study was conducted during 1994, which demonstrated the applicability of dual-band infrared thermal imaging to bridge decks. [22-25] We constructed small-scale surrogate bridge decks using concrete and asphalt-concrete slabs. Two nearly identical concrete test slabs were cast in January 1994. The slabs were 1.8 m (6 feet) square by 19 cm (7.5 inches) thick. During March 1994, one of the slabs was paved with a 5-cm (2-inch) thick layer of asphalt. These same slabs were used for the present study where we compared solar-heated thermal maps with flash-heated thermal inertia maps to characterize surrogate delaminations in concrete and asphalt-concrete slabs.

The synthetic delaminations were constructed with five 5-cm (2-inch) deep embedded pieces of Styrofoam cut to various square sizes and thicknesses. The Styrofoam pieces formed synthetic delaminations, at a depth of 5 cm in the unpaved concrete slab and 10 cm in the paved concrete slab. We placed objects on the slabs which produced surface clutter. During April 1994, we mapped surface temperature differences for paved and unpaved concrete slabs. Later, we developed image-processing methods to unmask synthetic delaminations and remove surface clutter. The temperature images were processed using the VIEW computer code developed at LLNL. [22-25]

We developed emissivity-corrected surface temperature maps to depict heat flow anomalies produced by subsurface delaminations and to remove surface clutter. Clutter is unwanted thermal detail. Clutter often occurs from foreign deck materials. Clutter sometimes occurs from uneven shade on the bridge deck surface. Clutter may also occur from unseen chemical differences in concrete which respond differently at the two IR wavelengths measured with the dual-scanner system. By mapping the DBIR image differences at 3-5 μm (SW), and 8-12 μm (LW), we identify and remove foreign material clutter.

We discovered a strong correlation between the defect volume, and the temperature signal which it produced. The daytime (above-ambient) minus nighttime (below-ambient) IR temperature-difference signals varied linearly with the volume of the embedded Styrofoam pieces which produced the temperature differences. Delaminated bridge decks with large volumes of damaged concrete are expected to produce larger daytime and nighttime temperature excursions when compared to those of delaminated bridge decks with small volumes of damaged concrete or when compared to normal bridge decks.

3. GRASS VALLEY CREEK BRIDGE INSPECTIONS

An actual bridge demonstration in 1996 "predicted" delaminated deck areas while driving over the Grass Valley Creek Bridges at 25 mph in the DBIR Bridge Inspection Van. Later, we confirmed our prediction with "bridge truth". Bridge truth is well-documented visual, photographic, and video-tape observations, which record the location and amount of damaged concrete while the bridge deck is rehabilitated. In the present study, we compared solar-heated thermal maps with flash-heated thermal inertia maps for characterizing surrogate delaminations in concrete and asphalt-concrete slabs.

We designed, built, tested and applied a mobile DBIR thermal imaging laboratory for bridge inspections.[26-28] This work was sponsored by the Federal Highway Administration (FHWA) Nondestructive Evaluation Research and Development Program. Results from our surrogate bridge deck demonstration guided the design of the mobile bridge-inspection system shown in Figure 1. The Agema 900 dual scanners, which had 40° lenses, were mounted on a telescoping mast about 4 meters (13 ft) above the roadway. The system controls, 12-bit digital image processor, and high-speed recording hard drives were inside the modified 27-foot motor home. The IR cameras scanned the reinforced-concrete bridge deck for subsurface defects called delaminations. The mobile DBIR laboratory is currently undergoing extensive testing to examine bridges by the FHWA.

We drove the self-contained mobile laboratory to the Grass Valley Creek Bridges near Redding, California where we acquired bridge-deck thermal images. Using thermal image analysis, we distinguished subsurface delaminations (concrete gaps), from surface materials and clutter (e.g. paint, patches, hinges and shaded areas). Shaded areas have thermal responses similar to subsurface delaminations during the day, but different thermal responses compared to subsurface delaminations at night.

To distinguish delaminated decks from normal decks, decks with surface material differences, and clutter, we determined the delamination site: (1) size, shape, relative volume and location; (2) thermal inertia (or daytime minus nighttime temperature differences) relative to ambient deck sites; (3) daytime and nighttime temperatures, relative to ambient deck sites; and (4) spectral (or LW - SW) image differences, relative to deck sites with surface material differences and clutter.

Figure 1. View of the mobile dual-band infrared (DBIR) thermal imaging laboratory as it inspects a Grass Valley Creek bridge near Redding California.[28] The DBIR laboratory's cameras are mounted on a telescoping mast about 4 m (13 ft) above the roadway. They scan the reinforced-concrete bridge deck for subsurface defects called delaminations.

During the day, delaminated deck sites were masked by variable shade from hills, trees, or cloud-cover. At night, delaminated deck sites were 0.5 °C cooler than normal deck sites, and shade was not a problem. Shade presents a special type of unwanted detail, or surface clutter. Shade affects the interpretation of bridge inspections, when the bridge is deep within a canyon and surrounded by hills and trees. Thermal inertia responses (i.e. daytime above-ambient minus nighttime below-ambient thermal difference patterns) distinguish delaminated deck sites with bulk material damage from shaded, but undamaged, deck sites.

To distinguish delaminated decks from normal decks, decks with foreign materials, and shaded decks, we studied the Grass Valley Creek bridge-deck images recorded and displayed using the Agema 900 System 12-bit digital image processor and display monitor. Using the VIEW signal and image processing code developed at LLNL, we analyzed a 0.76 m^2 (8.2 ft^2) delaminated deck site. See Figures 2, 3 and 4.

Figure 2 compares a digitized photo of the delamination site with shortwave (SW) and longwave (LW) infrared thermal images taken simultaneously with the video photo and a coregistered SW minus LW spectral difference image. Figure 3 shows the spectral difference image processed on the SGI workstation as a mask to remove nonthermal surface clutter, thereby clarifying subsurface delamination sites. Figure 4 compares the predicted delamination site with "bridge truth" photography of the delamination site after the pavement was removed. The thermal images were recorded during daytime, at 12:04 hrs on November 3 1995. The photos were taken in 1997, prior to removing the bridge deck for the scheduled bridge repairs.

Thermal mapping depicts normal decks, delaminated decks and clutter (unwanted detail associated with surface features). Clutter may result from thermal features (deck sites with uneven shade) or nonthermal features (foreign deck materials). Using LW - SW clutter masks, we can easily distinguish normal decks from delaminated decks after removing nonthermal clutter generated by foreign surface materials.

To distinguish delaminated decks from normal decks and decks with thermal clutter, such as uneven daytime shade, requires obtaining coregistered temperature-difference maps taken during the day and the night. Presently, it is not feasible to obtain coregistered daytime and nighttime temperature maps from the mobile bridge inspection van. In the next section, we describe a stationary DBIR system shown in Figure 5. This system maps thermal inertia variations from surrogate delaminations in flash-heated concrete and asphalt-concrete slabs. Thermal inertia maps are insensitive to thermal clutter.

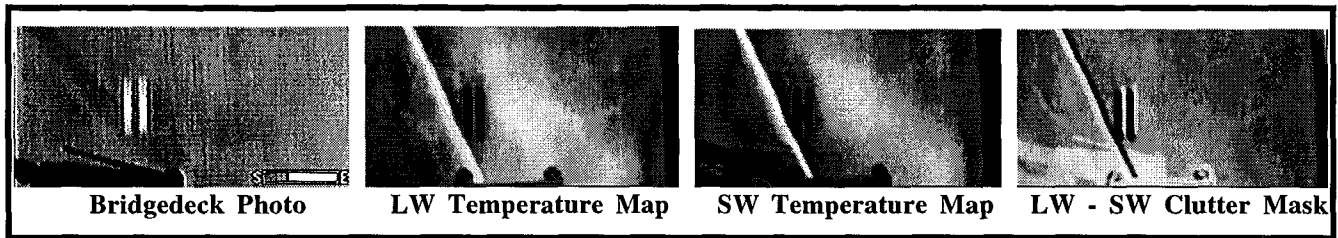| Bridgedeck Photo | LW Temperature Map | SW Temperature Map | LW - SW Clutter Mask |

Figure 2. The digitized Grass Valley Creek bridgedeck photo (far left), unlike the daytime LW - SW clutter mask (far right) is not coregistered with the longwave (LW) and shortwave (SW) IR daytime temperature maps shown left and right of center.

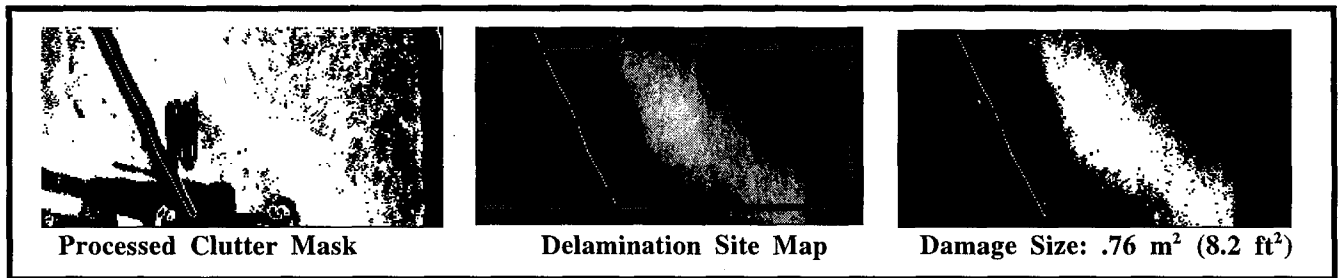| Processed Clutter Mask | Delamination Site Map | Damage Size: .76 m^2 (8.2 ft^2) |

Figure 3. The processed clutter mask (left) removes clutter from the shortwave IR temperature map to depict the subsurface delamination site (center). The delamination size (right) is determined using a computer program which counts the number of warmer-than-ambient pixels (picture elements) within the delamination site relative to the number of pixels for a known area.

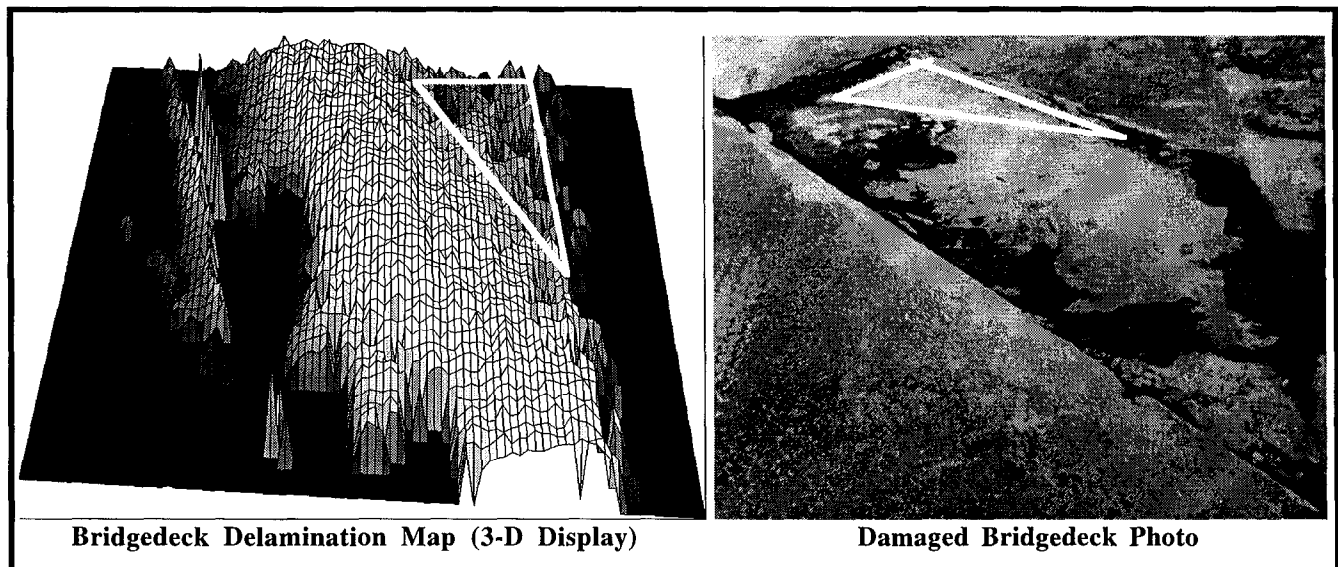| Bridgedeck Delamination Map (3-D Display) | Damaged Bridgedeck Photo |

Figure 4. The bridgedeck delamination map (left) uses the z coordinate to display daytime above-ambient and ambient temperatures, respectively for delaminated and normal deck areas, such as shown within the white triangle. After removing the pavement above the "predicted" delamination, we discovered 0.12 cubic meters (4.2 cubic feet) of damaged concrete. The white triangle on the "bridge-truth" photo (right) coincided with the predicted undamaged deck site. Also, the scalloped edge of the damaged bridge deck on the photo confirmed the predicted shape of damaged concrete on the bridgedeck delamination map.
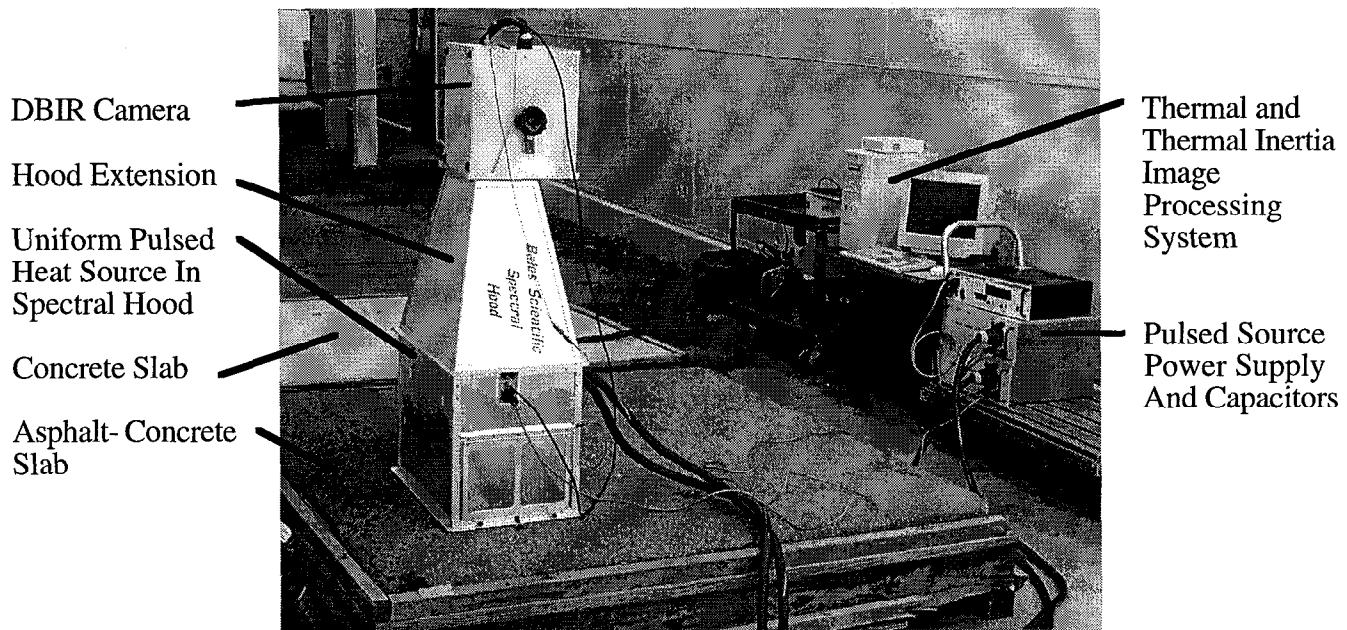
Figure 5. The Bales dual-band infrared (DBIR) camera, uniform 4ms pulsed heat source, spectral hood, and thermal image processing system were used in the above set-up to detect hidden Styrofoam implants in concrete and asphalt-concrete slabs.

4. THERMAL INERTIA MAPPING

Thermal inertia mapping is a tool for visualizing and quantifying subsurface defects. Physically, thermal inertia is a measure of the resistance of the bridge deck to temperature change. Experimentally, it is determined from the inverse slope of the surface temperature versus the inverse square root of time. Mathematically, thermal inertia is the square root of the product of thermal conductivity, density, and heat capacity.

Thermal nondestructive evaluation (NDE) currently specifies the location of structural defects in two spatial dimensions. Three dimensional spatial characterizations of defect types, volumes and depths require a unique approach to the detection, analysis and interpretation of thermal NDE. We call this approach IR computed tomography. Infrared computed tomography (IRCT) maps precise surface temperatures and bulk-material thermal inertias. Surface-temperature maps specify defect size and location. Thermal inertia maps provide information to specify defect thickness, depth and volume.

The rationale for thermal inertia mapping is based on the solution to the heat transfer equation for a thick target with an instantaneous surface heat flux, which is:[29,30]

$$T(x,t) = \frac{q}{\sqrt{4\pi k\rho c t}}\exp\left(-\frac{x^2}{4\alpha t}\right) \tag{1}$$

where T is temperature, x is depth beneath the surface, k is thermal conductivity, ρ is density, c is heat capacity, a is thermal diffusivity, t is time and q is the surface heat flux. For a semi-infinite solid approximation, the surface temperature is proportional to the inverse square root of time and inversely proportional to the thermal inertia, P, which varies as $(k\rho c)^{1/2}$.

The Lawrence Livermore National Laboratory entered into a cooperative reasearch and development agreement (CRADA) with Bales Scientific Inc. (BSI). BSI manufactures the dual-band IR camera, uniform flashlamp source and thermal image processing system. By teaming with Bales, we programmed the image processing system to map temporal variations in the slope of temperature versus the inverse square root of time. Using a dimensionless scale, we depicted percent variations in inverse thermal inertia for normal concrete and asphalt-concrete slabs, relative to concrete and asphalt-concrete slabs with Styrofoam implants. The implants behave like surrogate bridgedeck delaminations (or subsurface cracks from corroded rebars).

We applied a uniform 15 kilo-Joule, 4-ms pulsed heat load to stimulate internal defects; the Bales commercial dual-band infrared (DBIR) camera system to measure time-varying, defective-structure temperature and thermal inertia responses; and a computer tomography (CT) program to create evaluated defect maps, in near real time. The solar-heated concrete slab thermal maps in Figures 6 thru 9 are compared with flash-heated thermal inertia maps in Figure 9. The solar-heated asphalt-concrete thermal maps in Figure 10 are compared with flash-heated thermal inertia maps in Figure 11.

Dual-band infrared temperature-rise maps of a normal 1.5 ft x 1.0 ft flash-heated concrete slab section, taken at three different times after the flash are shown in Figure 6. The temperature rise decreases as the inverse square root of time after the flash as shown within the limits of experimental uncertainty in Figure 6. Temperature maps of a 4 ft x 4 ft concrete slab section heated naturally by the midday sun are shown in Figure 7. Small temperature differences apply for the LW (longwave), SW (shortwave), and dual-band infrared responses. Also, spectral differences occur for the silicate composition at the center of the concrete slab which produced an apparent temperature difference. This difference was associated with excitation of the 9-10 μm molecular resonance in the LW infrared band. Figure 8 tabulates the average spot temperatures at implant sites 1 thru 5 which are oriented on the concrete slab as shown by the diagram. The Styrofoam implant squares were 2 inches deep; 9 inches (#1), 6 inches (#2), and 4 inches (#3 thru #5) on-a-side; and 1/8 inch (#1 thru #3), 5/16 inch (#4), and 9/16 inch (#5) thick.

In Figure 9, the reinforced concrete slab temperature maps (top row) are compared with inverse thermal inertia maps (bottom row) for delamination sites #1 and #5. The 9 inch square implant had 8% $\pm$ 2% less thermal inertia, $P = (k\rho C_p)^{1/2}$ than the slab to the left of the implant at 1s to 15s after the heat flash. The 4 inch square implant had 6% $\pm$ 2% less thermal inertia than the slab to the left of the delamination at 1s to 15s after the heat flash. The #1 and #5 implant volumes were 10.1 and 9.0 cubic inches, respectively. Thus the thermal inertia decrease, a bulk volume effect, was about the same (7%) at each site.

Dual-band infrared temperature maps of the 6-ft asphalt-concrete slab, heated naturally by the midday sun, are shown in Figure 10. Nine-inch wide Styrofoam implants formed surrogate delamination sites which were 2 inches deep at the asphalt-concrete interface (#6, left) and 4 inches deep under asphalt-concrete (#1, right). There were no clear indications of the 4 inch deep implants #2 thru #5 which were oriented at locations comparable to those shown in Figure 8.

In Figure 11, the asphalt-concrete slab temperature maps (top row) were compared with inverse thermal inertia maps (bottom row) of delamination sites #6 and #1. The 2-inch deep delamination had 8% $\pm$ 3% less thermal inertia, $P = (k\rho C_p)^{1/2}$ than the slab left of the delamination at 16s to 24s after the heat flash. The 4-inch deep delamination had 6% $\pm$ 3% less thermal inertia than the slab left of the delamination at 16s to 24s after the flash.

Like delaminated bridge structures, flash-heated alphalt-concrete and concrete slabs with Styrofoam implants have less heat capacity (less thermal inertia) and heat up (or cool off) faster than normal deck materials. The inverse thermal inertia signal for a void, air gap or delaminated area is 287 times larger than the comparable signal for an equal volume of concrete. We note the inverse thermal inertia signal increase, or thermal inertia signal decrease, relative to the host materials for similar-volume implants at 2-inch depths in concrete, and at 2-inch and 4-inch depths in asphalt-concrete were all approximately 7%.

The slab temperature maps depict implants with degraded sizes from thermal smear, whereas the slab inverse thermal inertia maps depict implants 5 cm and 10 cm deep without implant size degradation. We imaged slab surface temperatures, and temperature differences before and after the flash, and slab material inverse thermal inertias at .5s $\pm$ .4s, 8s $\pm$ 7s, and 20s $\pm$ 4s.
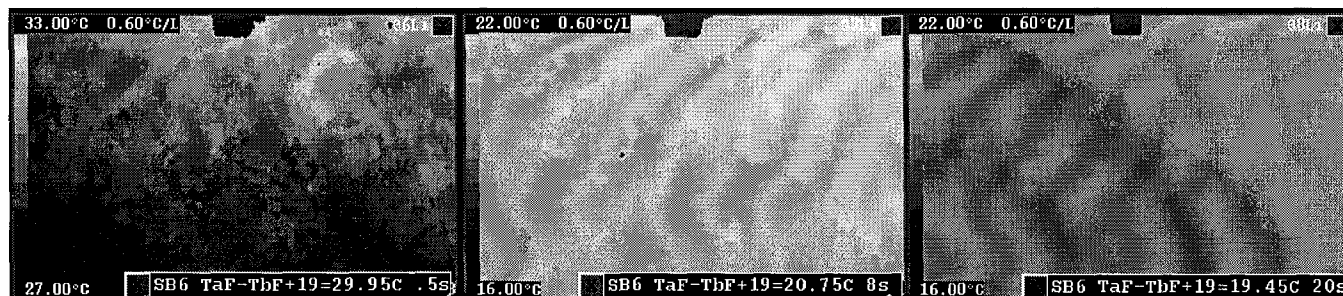

Figure 6. Flashlamp-related concrete slab temperature rises averaged 11.0 °C at .5s $\pm$ .4s (left), 1.75 °C at 8s $\pm$ 7s (center) and .45 °C at 20s $\pm$ 4s (right) after the flash for the 1.5 ft x 1.0 ft section of reinforced concrete slab which had no Styrofoam implants.

8-12 μm LW   3-5 μm SW   0.5 (LW+SW)   LW-SW+36 °C
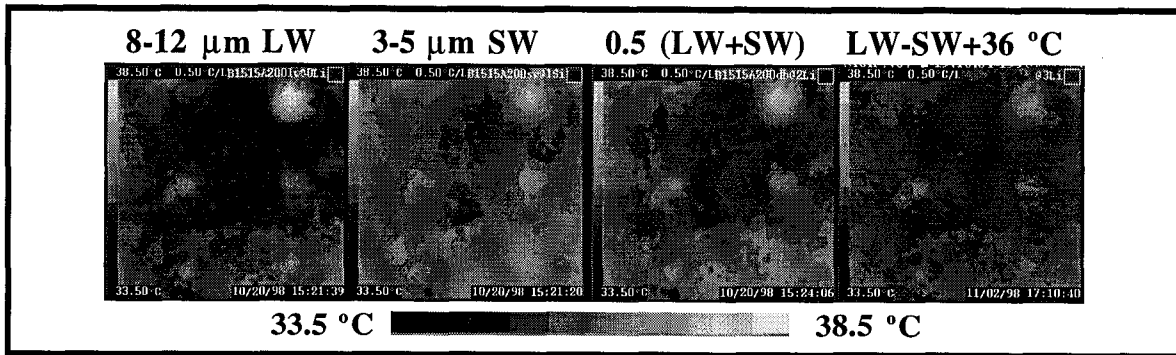
33.5 °C ▬▬▬▬▬ **38.5 °C**

Figure 7. Temperature maps of 4-ft concrete slab section. Temperature differences occur for the LW, SW, dual-band (DB) infrared and spectral difference responses near the slab center where the silicate composition excites a LW molecular resonance.

Site	LW	SW
1Av	38.25	37.55
2Av	36.55	36.50
3Av	37.05	36.75
4Av	36.40	36.40
5Av	36.70	36.50

5	1
	2
4	3

Site	.5(LW+SW)	LW-SW+36
1Av	37.85	36.80
2Av	36.55	36.05
3Av	36.85	36.30
4Av	36.35	36.00
5Av	36.60	36.20

Figure 8. Average temperatures (°C) and orientations of 5 surrogate concrete delaminations. Styrofoam implant squares were 2 inches deep; 9 (#1), 6 (#2), and 4 (#3 thru #5) inches on-a-side; and 1/8 (#1 thru #3), 5/16 (#4), and 9/16 (#5) inches thick.

Implant #1, 9 inch square, 2 inch depth   Implant #5, 4 inch square, 2 inch depth

33.5 °C ▬▬▬▬▬ **38.5 °C   33.5 °C** ▬▬▬▬▬ **38.5 °C**

90 % ▬▬▬▬▬ **110 %   90 %** ▬▬▬▬▬ **110 %**
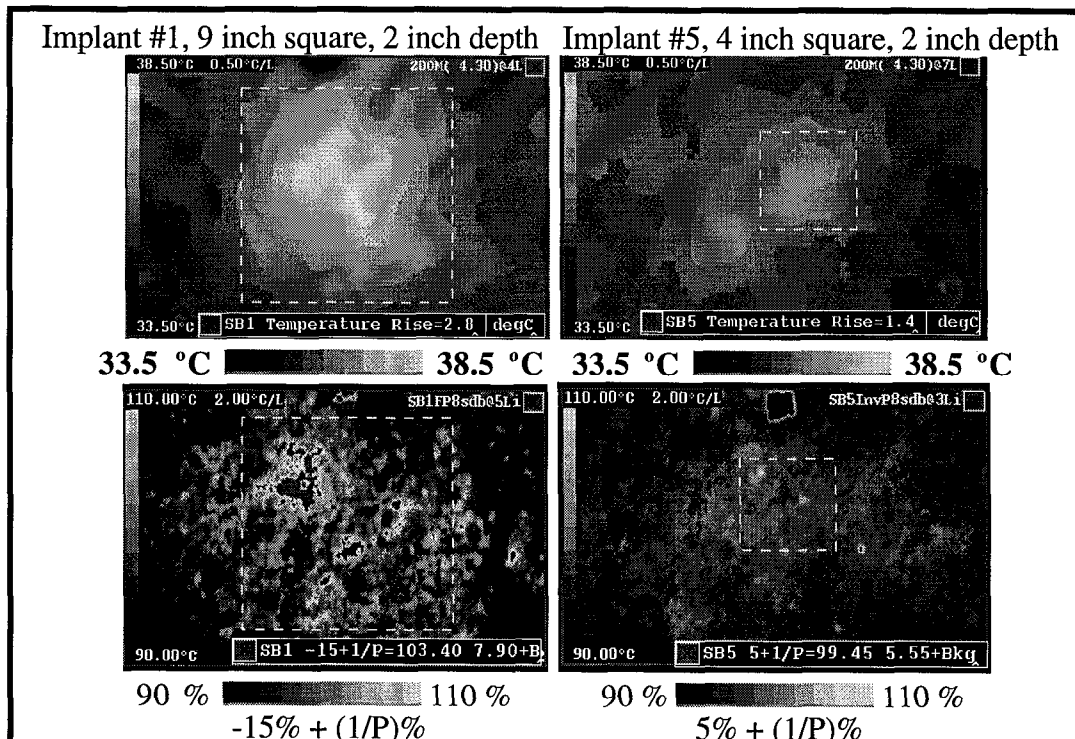
-15% + (1/P)%   5% + (1/P)%

Figure 9. Reinforced concrete slab temperature maps (top row) compared with inverse thermal inertia maps (bottom row) for delamination sites #1 and #5. The 9 inch square implant had 8% $\pm$ 2% less thermal inertia, $P = (k\rho C_p)^{1/2}$ than the slab to the left of the implant at 1s to 15s after the heat flash. The 4 inch square implant had 6% $\pm$ 2% less thermal inertia than the slab to the left of the delamination at 1s to 15s after the heat flash.
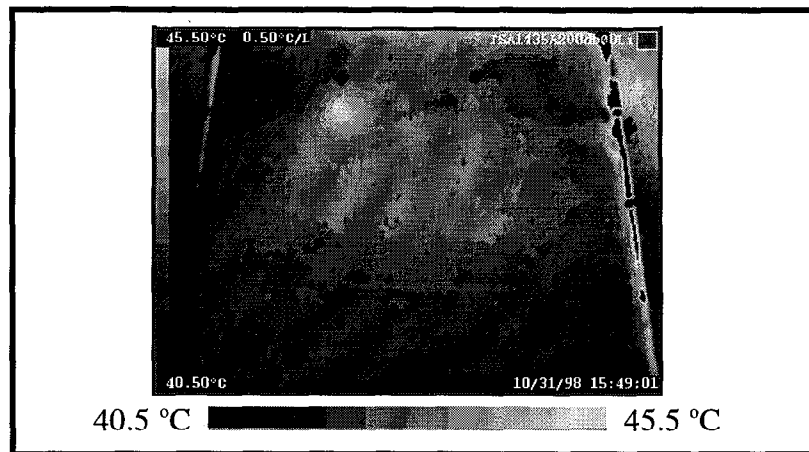
Figure 10. Dual-band infrared temperature map of the 6-ft asphalt-concrete slab. Nine-inch wide Styrofoam implants formed surrogate delamination sites which were 2 inches deep at the asphalt-concrete interface (#6, left) and 4 inches deep under asphalt-concrete (#1, right).
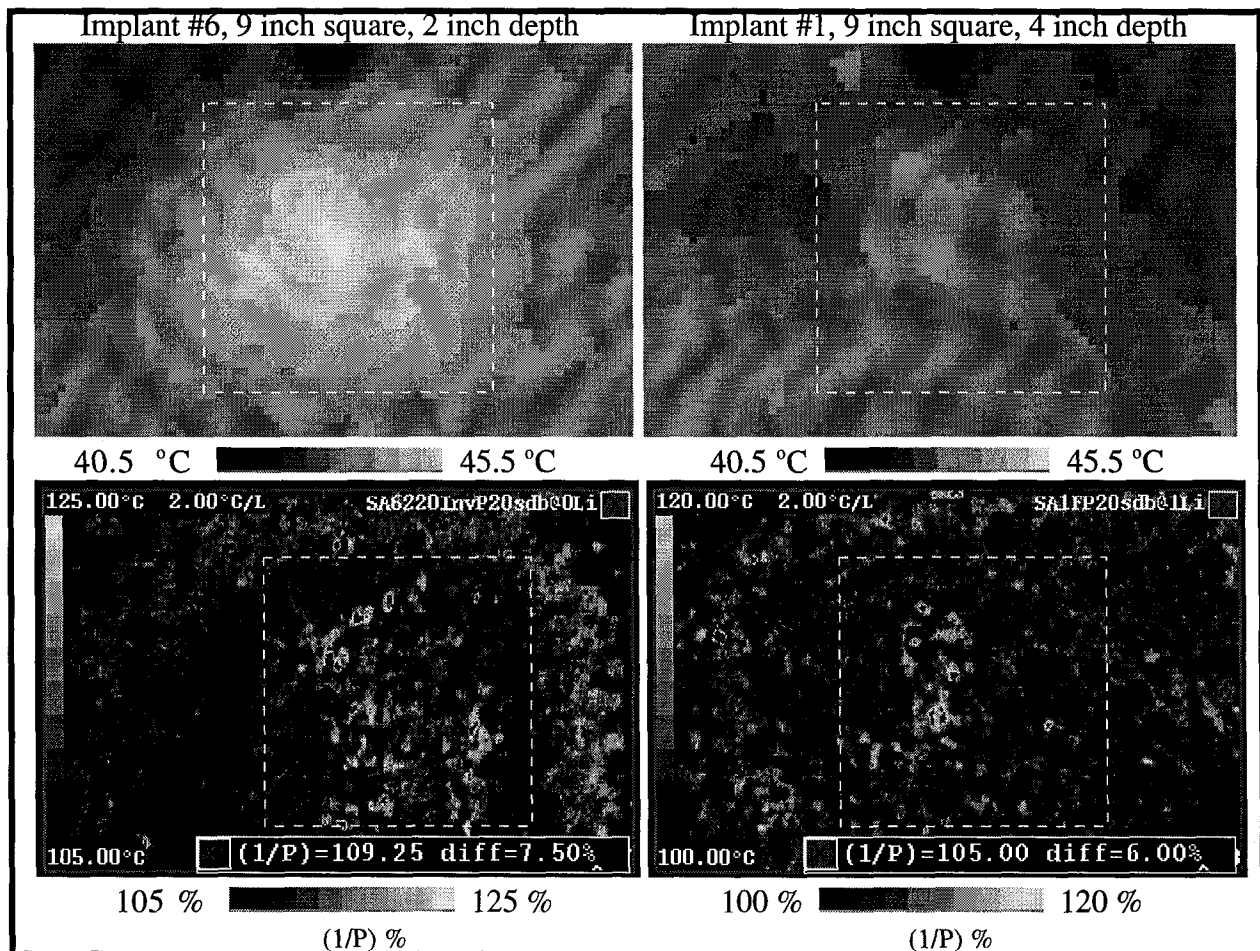

Figure 11. Asphalt-concrete slab temperature maps (top row) compared with inverse thermal inertia maps (bottom row) of delamination sites #6 and #1. The site #6, 2-inch deep delamination had 8% $\pm$ 3% less thermal inertia, $P = (k\rho C_p)^{1/2}$ than the slab left of the delamination at 16s to 24s after the heat flash. The site #1, 4-inch deep delamination had 6% $\pm$ 3% less thermal inertia than the slab left of the delamination at 16s to 24s after the flash.

After the flash, concrete and asphalt-concrete slab thermal inertias had sufficient contrast to detect 2-inch (5-cm) deep and 4-inch (10-cm) deep surrogate delaminations at times as fast as .5s ± .4s, 8s ± 7s and 20s ± 4s. Thermal diffusion from solar heating is believed to be a slow process. Measurements of 2-inch deep buried land mines [9-13] indicated the solar peak temperature was delayed 20 or 30 minutes in sand, at a depth of 2 inches. We believe the 4ms flashlamp pulse may heat the slab interior faster, enabling us to detect deeper delaminations than is possible with solar heating as the only heat source.

Another source of heating within the interior of the slab is absorption of acoustic energy. The sudden heating of the slab surface generates an acoustic pulse which propagates through the material. Part of this pulse is absorbed within the material causing a slight temperature rise. The distribution of the absorption and its effect on the surface temperature-time history would be modified by inhomogeneities within the slab. This could conceivably cause rapid measurable variations of inverse thermal inertia from deeply buried implants or delaminations. Further theoretical and computational work would be needed to estimate the magnitude of this effect. A theoretical description of this thermoelastic effect can be found in the text by Achenbach [31] and in the doctoral thesis by James Spicer [32].

5.0 SUMMARY AND CONCLUSION

We analyzed a delamination detected with the mobile DBIR bridge inspection laboratory at limited highway speeds over 0.4 lane miles of Grass Valley Creek bridge decks. The distinction between defective deck sites (with structural damage from subsurface delaminations) and normal but cluttered deck sites (with foreign surface materials or uneven shade) was based on their respective spatial, spectral, thermal, thermal inertia, emissivity and temporal responses.

We depicted foreign surface materials which had the wavelength-dependent emissivity behavior of a selective radiator source. Examples of these foreign surface materials include: painted lanes, aluminum-tape markers, pavement contamination, patches, expansion joints, and materials with compositions unlike the host deck material. These surface features were clearly depicted on LW (8-12 μm) minus SW (3-5 μm) spectral difference maps. Once identified, these surface features are removed from the LW and SW apparent temperature maps to clearly identify delaminations.

The DBIR method replaces human speculation about bridge deck emissivity behavior, based on visible observation, with spectral measurement. This allows identification and subsequent removal of unwanted surface features to clarify interpretation of bridge deck delaminations. By clarifying interpretation of delaminations, we improve bridge inspection reliability. We demonstrated that the spectral response difference for the longwave and shortwave bands removed non-thermal clutter from foreign materials on the bridge deck, but not thermal clutter from sites with variable shading from the sun.

Thermal inertia mapping has the potential to distinguish delaminated deck sites from deck sites shaded by hills, trees and cloud-cover. Thermal inertia was previously studied by conducting daytime and nighttime inspections of the Grass Valley bridge delaminations from the mobile DBIR bridgedeck inspection van. The 2.9 °C ± 0.4 °C average day-night temperature difference for a delaminated Grass Valley Creek bridgedeck area was comparable to the 3.6 °C ± 0.6 °C day-night temperature difference for the 9-inch square, 1/8-inch thick, synthetic delamination in the concrete slab, both of which were reported previously. [26,28] The synthetic and natural delaminations had about the same thermal inertia, or resistance to temperature change, which was less than the thermal inertia for normal, undamaged decks.

We were unable to coregister daytime and nighttime thermal images recorded from the mobile DBIR bridgedeck inspection van as it crossed the bridge lane at approximately 25 mph. To better understand the feasibility of thermal inertia mapping for delamination detection, we flash heated concrete and asphalt-concrete slabs from a stationary platform. We processed thermal inertia maps depicting Styrofoam implants in concrete and asphalt-concrete slabs. The thermal inertia maps detected surrogate delaminations on 1.5 ft x 1.0 ft image frames. The solar-heated, implant-site thermal images were subject to lateral heat transfer (thermal smear). The flash-heated, implant-site thermal inertia images depicted the bulk material differences, from normal gravel to implants as deep as 2 and 4 inches within the concrete and asphalt-concrete slabs, without size degradation.

Dual-band infrared thermal and thermal inertia mapping provides an enabling technology for rapid, reliable, bridge deck inspections, while minimizing lane closures. The DBIR methods can indicate the fractional area of the bridge that is delaminated as well as locate and characterize the damaged regions. Flash-heated stationary systems play an important role to clarify interpretation of suspect delaminations by ruling out clutter from deck sites shaded by hills, trees and cloud-cover.

6. ACKNOWLEDGMENTS

7. REFERENCES

1. Richard P. Joyce, "Rapid Non-Destructive Delamination Detection" *U. S. Department of Transportation, Federal Highway Administration Report No. FHWA/RD85/051, Final Report Appendix B: Infrared Thermography-Summary Report.*, Apr. 1985.

2. Kenneth R. Maser, "New Technology For Bridge Deck Assessment, *U. S. Department of Transportation, Federal Highway Administration, Phase I Report No. FHWA-NETC-89-01.* Sept 1989.

3. Kenneth R. Maser, "New Technology For Bridge Deck Assessment", *U. S. Department of Transportation, Federal Highway Administration, Phase II Report No. FHWA-NETC-90-01.* May 1990.

4. D. G. Manning, and F. B. Holt, "Detecting Deterioration in Asphalt-Covered Bridge Decks," *Transportation Research Record No. 899,* Transportation Research Board, Washington D. C., pp. 10-20, 1983.

5. N. K. Del Grande, "Method for Identifying Anomalous Terrestrial Heat Flows"; *Patent No. 4,005,289,* Jan. 1977.

6. N. K. Del Grande, P. F. Durbin, K. W. Dolan, and D. E. Perkins, "Emissivity Corrected Infrared Method For Imaging Anomalous Structural Heat Flows", *Patent No. 5,444,241,* Aug. 22, 1995.

7. N. Del Grande, "Airborne and Field Temperature Surveys Compared At Long Valley KGRA, California", *Geothermal Resources Council Transactions 5,* p. 71, 1978.

8. N. K. Del Grande, "Airborne Temperature Survey Maps of Heat Flow Anomalies for Exploration Geology", *Proceeding of International Symposium on Remote Sensing of Environment, Second Thematic Conference on Remote Sensing for Exploration Geology,* Dec. 1982. Reprinted in Geothermal Resources Council Bulletin 14, p.3, 1985.

9. N. K. Del Grande, G. A. Clark, P. F. Durbin, D. J. Fields, J. E. Hernandez and R. J. Sherwood, "Buried Object Remote Detection For Law Enforcement", *Surveillance Technologies, SPIE Vol. 1479,* p. 335, 1991.

10. N. K. Del Grande, "Temperature Evaluated Mine Position Survey (TEMPS) Application of Dual Band Infrared Methodology", *Proceedings of the 1990 Meeting of the IRIS Specialty Group on Passive Sensors,* IRIA/ERIM sponsored symposium, 1990.

11. N. K. Del Grande, "Sensor Fusion Methodology for Remote Detection of Buried Land Mines", *Proceedings of the 3rd National Symposium on Sensor Fusion,* Orlando, Fl, Vol. 1, IIAC/ERIM, p.407, 1990.

12. N. Del Grande, "Airborne Detection Of Buried Minefields", *Energy and Technology Review,* University of California LLNL Report, UCRL-52-000-91-12,9, 1991.

13. N. K. Del Grande, P. F. Durbin, M. R. Gorvad, D. E. Perkins, G. A. Clark, J. E. Hernandez and R. J. Sherwood, "Dual-band Infrared Capabilities for Imaging Buried Object Sites", in *Proceedings of SPIE Conference 1942: [1]Underground and Obscured Object Imaging and Detection,* Ed. N. Del Grande, I. Cindrich and P. Johnson, Orlando FL, pp. 166-177, Apr. 1993.

14. G. A. Clark, J. E. Hernandez, S. K. Sengupta, R. J. Sherwood, P. C. Schaich, M. R. Buhl, R. J. Kane, M. J. Barth, N. K. Del Grande, "Sensor Feature Fusion for Detecting Buried Objects", in *Proceedings of SPIE Conference 1942: Underground and Obscured Object Imaging and Detection*, Ed. N. Del Grande, I. Cindrich and P. Johnson, Orlando FL, Apr. 1993.

15. N. K. Del Grande, P. F. Durbin and D. E. Perkins, "Dual-Band Infrared Imaging Applications: Locating Buried Minefields, Mapping Sea Ice and Inspecting Aging Aircraft", *Review of Progress in Quantitative Nondestructive Evaluation Vol. 12*, Ed. by D. O. Thompson and D. E. Chimenti, Plenum Press, NY, 1993.

16. N. K. Del Grande, K. W. Dolan, P. F. Durbin, M. R. Gorvad, B. T. Kornblum, D. E. Perkins, D. J. Schneberk and A. B. Shapiro, "Three-dimensional dynamic thermal imaging of structural flaws by dual-band infrared computed tomography", in *Proceedings of SPIE Conference 1942: Underground and Obscured Object Imaging and Detection*, Ed. Nancy Del Grande, Ivan Cindrich and Peter Johnson, Orlando FL, pp. 207-215, Apr. 1993.

17. N. K. Del Grande, K. W. Dolan, P. F. Durbin, M. R. Gorvad and A. B. Shapiro, "Dynamic thermal tomography for nondestructive inspection of aging aircraft", in *Proceedings of SPIE Conference 2001: Nondestructive Inspection of Aging Aircraft*, Ed. Michael Valley, Albert Kobayashi and Nancy Del Grande, San Diego CA, pp. 66-77, July 1993.

18. N. K. Del Grande, "Dual-Band Infrared Imaging for Quantitative Corrosion Detection in Aging Aircraft", *Proceedings of the American Society for Nondestructive Testing (ASNT) Meeting*, Long Beach CA, Nov. 1993.

19. N. K. Del Grande and P. F. Durbin, "Dual-band infrared imaging to detect corrosion damage within airframes and concrete structures", in *Proceedings of SPIE Conference 2245: Thermosense XVI: An International Conference on Thermal Sensing and Imaging Diagnostic Applications*, Ed. John R. Snell, Jr., Orlando FL, pp. 202-209, Apr. 1994.

20. Nancy K. Del Grande and Philip F. Durbin, "Multi-use applications of dual-band infrared (DBIR) thermal imaging for detecting obscured structural defects", in *Proceedings of SPIE Conference 2217A: Underground and Obscured Object Imaging and Detection*, Ed. Nancy Del Grande, Ivan Cindrich and Peter Johnson, Orlando FL, pp. 107-116, Apr. 1994.

21. N. K. Del Grande and P. F. Durbin, "Mapping hidden aircraft defects with dual-band infrared computed tomography", in *Proceedings of SPIE Conference 2455: Nondestructive Evaluation of Aging Aircraft, Airports, Aerospace Hardware, and Materials*, Ed. Tobey Cordell, Oakland CA, pp. 82-93, June 1995.

22. Nancy K. Del Grande and Philip F. Durbin, "Stimulated dual-band infrared computed tomography: a tool to inspect the aging infrastructure", in *Proceedings of SPIE Conference 2552: Infrared Technology XXI*, Ed. Bjorn F. Andreson and Marija S. Scholl, San Diego CA, pp. 292-301, July 1995.

23. Nancy K. Del Grande and Philip F. Durbin, "Precise Thermal NDE For Quantifying Structural Damage", in *Review Of Progress In Quantitative Nondestructive Evaluation, Volume 15A*, Ed. by Donald O. Thompson and Dale E. Chimenti, Plenum Press, New York, pp. 525-531, 1996.

24. Philip Durbin and Nancy Del Grande, "Dual-Band Infrared Imaging For Concrete Bridge Deck Inspection", *Proceedings of Structural Materials Technology-An NDT Conference*, Atlantic City NJ, Feb. 1994.

25. N. K. Del Grande and P. F. Durbin, "Using emissivity-corrected thermal maps to locate deep structural defects in concrete bridge decks", in *Proceedings of SPIE Conference 2456: Nondestructive Evaluation of Aging Bridges and Highways*, Ed. Steve Chase, Oakland CA, pp. 250-261, June 1995.

26. Philip F. Durbin, N. K. Del Grande, and Paul C. Schaich, "Demonstration of Dual-Band Infrared Thermal Imaging for Bridge Inspection", Phase II Final Report, Order No. DTFH61-93-Y-00145, Federal Highway Administration Nondestructive Evaluation Research and Development Program, UCRL-CR-123341, March 1996.

27. N. Del Grande, "Dual-Band Infrared Computed Tomography: Searching for Hidden Defects", *Science and Technology Review*, University of California LLNL Report, UCRL-52000-96-5, p. 23, May 1996.

28. Nancy K. Del Grande, Philip F. Durbin, Clint M. Logan, Dwight E. Perkins and Paul C. Schaich, "Demonstration of dual-band infrared thermal imaging at Grass Valley Creek Bridges", in *Proceedings of SPIE Conference 2946: Nondestructive Evaluation of Bridges and Highways*, Ed. Steve Chase, Scottsdale, AZ, pp. 166-177, Dec. 1996.

29. H. S. Carslaw and J. C. Jaeger, *Conduction of Heat in Solids, 2nd Edition*, Oxford Univ. Pr., London, England. pp. 101, 112, and 259, 1980.

30. Jane W. Maclachlan Spicer, "Thermographic NDT", *SPIE Short Course Notes, SC37, Thermosense '93*, Orlando Fl. Section 5, p. 13, 1993.

31. J. D. Achenbach, *Wave Propagation in Elastic Solids,* North-Holland Publishing Co., New York, 1973

32. James Spicer, *Laser Ultrasonics in Finite Structures: Comprehensive Modeling with Supporting Experiment,* Ph.D. dissertation, The Johns Hopkins University, 1991.